Appl. Phys. A 87, 419–425 (2007)
DOI: 10.1007/s00339-007-3906-z

Applied Physics A
Materials Science & Processing

D. SANDER✉
J. KIRSCHNER

Cantilever stress measurements of ferromagnetic monolayers

Max-Planck-Institut für Mikrostrukturphysik, Weinberg 2, 06120 Halle, Germany

Received: 24 August 2006/Accepted: 11 December 2006
Published online: 10 March 2007 • © Springer-Verlag 2007

ABSTRACT This overview summarizes important aspects of the cantilever stress measurement technique and its application to measurements of adsorbate-induced surface stress changes and magnetization-induced magnetoelastic stress (also called magnetostrictive stress) of ferromagnetic monolayers. The application of the cantilever technique as a torque magnetometer with monolayer sensitivity is demonstrated. The stress measurements indicate a correlation between surface stress changes and surface reconstruction, and they also identify the often decisive role of the magnetoelastic anisotropy for the non-bulklike magnetic anisotropy of ferromagnetic monolayers.

PACS 68.35.Gy; 68.35.Bs; 75.70.Ak; 75.80.+q

1 Introduction – how surface stress measurements started in Jülich, and how we incorporated magnetism-induced stress in Halle

When one of the authors, D.S., worked with H. Ibach at the IGV in Jülich as a diploma student in 1988, H. Ibach proposed to him to set up an experiment for his Ph.D. work to measure adsorbate-induced surface stress changes, and D.S. gladly accepted this offer. This marks the beginning of surface stress measurements in Harald Ibach's institute in Jülich.

Our short review summarizes some experimental aspects of the technique, and how we advanced it at the Max-Planck-Institut in Halle for the measurement of magnetic properties of monolayers, like magnetoelastic coupling and magnetic moment. This contribution shows with few selected examples what can be learned from stress measurements. The reader is referred to numerous review articles [1–9], Ph.D. theses [10–15], and data compilations [16] to gain a more comprehensive overview of this field.

1.1 *Surface stress measurements, why?*

Why are we interested in stress measurements at surfaces and in films? The measurement of film stress by the stress-induced curvature of a thin substrate dates back to the pioneering work by Stoney in 1909 [17], who related substrate curvature with film stress. Stress measurements have been performed ever since on rather thick films in the thickness range of several ten to hundreds of nanometers, where mainly bulklike properties of the deposited materials have been probed. Therefore one might wrongly assume, that stress measurements are old, established techniques, which cannot offer new insights to current surface science and nanomagnetism issues.

However, the advance of the detection techniques to monitor substrate curvature, e.g., highly sensitive capacitance [10, 18, 19] and optical beam deflection techniques [8, 20], improves the sensitivity of the substrate curvature measurement by several orders of magnitude, and a radius of curvature as large as several 100 km (corresponding to substrate deflections in the 0.1 nm range) can be safely determined. This corresponds to the detection of adsorbate-induced stress changes in the sub-monolayer coverage range, or to the detection of minute magnetoelastic stress in monolayer thin ferromagnetic layers.

The relevance and importance of stress measurements with sub-monolayer sensitivity can be clearly indicated by the following examples:

1. The electronic origin of surface stress and the adsorbate-induced change of surface stress have not yet been clearly elaborated in both theory and experiments [1, 2, 21–23]. It seems that the calculation of forces in the surface layer of a solid has attracted much less attention than the calculation of structural details like surface relaxation and adsorbate bonding geometry. One should strive for a detailed understanding of the relevant processes which govern stress at surfaces, as the quality of ab initio based calculations could be judged also with respect to a comparison between calculated and measured stress values. Also, several surface reconstructions have been discussed in terms of surface stress changes upon reconstruction in order to investigate a possible connection between the two. There is just limited experimental and theoretical work available, which deals with the role of surface stress for surface reconstruction.
2. The measurement of magnetization-induced stress in ferromagnetic layers gives quantitative values for the relevant magnetoelastic coupling coefficients [5]. Thus, the role of lattice strain for the resulting magnetic anisotropy of monolayer thin films and nanostructures can be explored. Measurements clearly show that the magnetoelastic coupling of these structures deviate sharply from its bulk be-

✉ Fax: +49-345-5511-223, E-mail: sander@mpi-halle.mpg.de

havior. The ab initio based theoretical description of these findings, which are essential for the discussion of magnetic anisotropy, are highly demanding, and only qualitative, but not quantitative, agreement between experiment and theory has been obtained [24, 25]. There is demand for both more experimental and theoretical work on this topic, which is also of high relevance for potential applications of ferromagnetic nanostructures.

The next section, Sect. 2, describes a capacitance and an optical two-beam technique to measure stress-induced substrate curvature. The following section describes applications of the technique to measure adsorbate-induced surface stress changes during oxygen adsorption on Cu(001), and the results are discussed in view of the O-induced missing-row reconstruction of Cu(001). Then we present data on the nonbulklike magnetoelastic coupling of ferromagnetic monolayers, where our stress measurements indicate that lattice strain modifies the magnetoelastic properties. The last section demonstrates that the magnetization induced torque of a cantilever sample in an external magnetic field can be successfully applied to measure quantitatively the magnetic moment of ferromagnetic monolayers.

2 Cantilever bending technique

Cantilever stress measurements exploit that any stress change at one of the surfaces of a thin substrate will induce a substrate curvature in proportion to the stress imbalance between front and backside of the substrate [26]. Thus, measurements of the curvature change of a substrate give quantitative values for the underlying stress change. The relation between stress change $\Delta\tau = \Delta(\tau_f t_f)$ and curvature change $\Delta(1/R)$ is given by the modified Stoney equation, which describes free two-dimensional bending due to a biaxial stress state $\Delta\tau = \Delta(\tau_f t_f) = Y_s {t_s}^2 \Delta(1/R)/(6(1-\nu_s))$, where the Young modulus and the Poisson ratio of the substrate are given Y_s and ν_s, respectively. The substrate thickness is given by t_s, and τ_f and t_s are the film stress and the film thickness. For a discussion of the applicability of this equation with regard to substrate clamping, crystalline anisotropy and anisotropic stress states the reader is referred to the references [27, 28].

To illustrate the demand for thin substrates we mention that in order to obtain a detectable curvature change, i.e., radius of curvature R smaller than a few km, one needs a thickness preferably below 0.5 mm. This enables the measurement of typical surface stress changes in the monolayer coverage regime, which are of the order of 1 N/m. Measurement on monolayer-induced stress changes were initially performed on Si substrates, where thin substrates were readily available. The demand for thin single crystalline metallic substrates presents a significant challenge for the crystal preparation, and rectangular single crystals of approximate dimensions 12 mm (length), 2.5 mm (width), and 0.1 mm (thickness) can be prepared in Jülich and Halle, and are also commercially available [29, 30].

We describe two established techniques to detect stress-induced curvature changes on single crystalline substrates, which are both illustrated in Fig. 1. One is based on the measurement of the curvature-induced change of distance between the substrate and a reference electrode, which is detected via the corresponding change of capacitance between the substrate and a reference electrode. The other method is based on an optical laser beam deflection set-up.

Highly sensitive fully automatic capacitance bridges are available [19] to detect the curvature-induced deflection of the substrate by measuring the corresponding capacitance change. The benefit of this method is that the sensitivity of the set-up for the detection of small deflections depends on the initial capacitance, which can be adjusted by changing the spacing between the substrate and the reference electrode. Typically, the initial capacitance is in the pF (10^{-12}) range, and capacitance changes as small as aF (10^{-18}) can be detected. This initial capacitance corresponds roughly to an electrode area of 1 cm^2 at an electrode spacing of 0.1 mm. The electrode area of roughly 1 cm^2 requires pretty large substrates, or alternatively a smaller substrate can be enlarged by mounting a proper sheet metal to it. Large Si substrates are available, and for single crystalline metal substrates a composite of the single crystal substrate and a sheet metal has been employed successfully.

The optical laser beam deflection technique exploits the reflection of one, two, or several, laser beams from the substrate surface onto a position-sensitive photo detector. A curvature change of the substrate induces a change of the position signal from which the curvature is calculated. The initial surface stress measurements on Si substrates were performed by optical deflection techniques [31, 32], and position sensitive detectors were available from the atomic force microscopes (AFM), where split photodiodes were used to monitor the cantilever deflection.

Both the capacitance and the optical beam deflection technique have been used successfully to investigate different

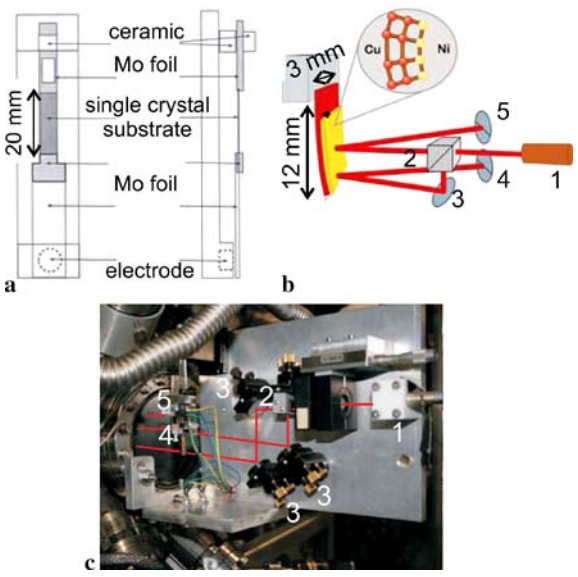

FIGURE 1 Schematic of the capacitance curvature detection (**a**) [12] and the optical beam deflection set-up (**b**) [9]. (**a**) The single crystalline sample is clamped between two Mo sheet metals, which serve as holding strip (*top*), and as sample electrode (*bottom*). This composite sample holder is mounted to the UHV manipulator. (**b**) The sample is mounted at its top end to the UHV manipulator, the bottom end is free. 1: laser, 2: beam splitter, 3: mirrors for beam alignment, 4, 5: position sensitive detectors. (**c**) Photograph of the set-up, mounted directly to an UHV CF-100 window-flange, numbers as in (**b**)

aspects of adsorbate-induced stress, film stress and magnetoelastic stress [5, 8]. In hindsight it seems that main advantages of the optical set-up are that less specialized sample holders are required in UHV (e.g., no electrical connections), as only the sample, and not the optics, are within the vacuum chamber. Also, multiple beam measurements enable a direct detection of the curvature, possibly along different directions. This facilitates the quantitative data analysis substantially. This is due to the reduced impact of the substrate clamping on the stress-induced curvature as compared to the stress-induced deflection [27].

3 Adsorbate-induced surface stress and surface reconstruction

One important incentive to start surface stress measurements in Jülich was to investigate experimentally the correlation between adsorbate-induced surface stress changes and surface reconstruction [10]. The surface stress change upon the C-induced p4g reconstruction of Ni(001) was measured. The results indicated a C-induced increase of compressive stress with C-coverage, where the stress increase ceased upon the onset of the p4g-reconstruction (clock reconstruction). Thus, these early experiments suggested a direct link between adsorbate-induced compressive surface stress and reconstruction. But does the surface stress change drive the reconstruction? Surface stress measurements alone are not sufficient to answer this question. However, in conjunction with earlier phonon dispersion measurements the results indicate that the C-induced p4g reconstruction is of the soft phonon type, and it seems appropriate to ascribe this reconstruction to the C-induced compressive surface stress [1, 33, 34].

Recently we have studied the O-induced missing row reconstruction of Cu(100) in a combined experimental and theoretical effort [23]. In contrast to the p4g reconstruction mentioned above, where the surface atoms are laterally displaced into new positions of the reconstructed phase, here every fourth row of surface atoms is ejected from the surface layer upon reconstruction.

Our stress measurements of Fig. 2 indicate a compressive surface stress change upon O-exposure of $-0.6\,\mathrm{N/m}$ at 500 K, which induces the missing row reconstruction, and $-1.0\,\mathrm{N/m}$ at 300 K for the c(2 × 2) structure. Additional measurements revealed that for both cases the

O-saturation coverage is 0.5, and we conclude that the missing row reconstruction leads to a smaller O-induced compressive surface stress change as compared to the c(2 × 2) phase.

Does this finding indicate that surface stress drives the O-induced missing row reconstruction? This cannot be judged from the experimental data alone. The reason is that the stress measurements reveal an O-induced stress change. However, as the total energy of the reconstructed phase needs to be lower than that of the metastable c(2 × 2) phase, it is the absolute surface stress, i.e., the magnitude of the surface stress – irrespective of its sign – which matters here. This notion is corroborated by calculations which indicate a parabolic relation between the energy per surface atom (*y*-scale) and surface strain (*x*-scale). The surface stress is given by the slope of this curve, and therefore a smaller surface stress magnitude can be correlated with a lower energy per surface atom.

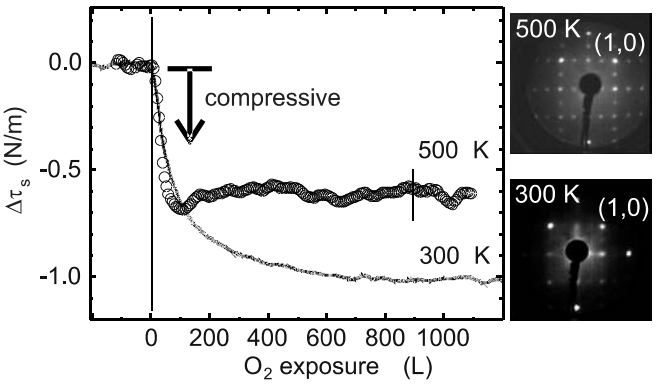

FIGURE 2 Oxygen-induced surface stress change during O-exposure of Cu(100) at 500 and 300 K. The *insets* show the low-energy electron diffraction (LEED) pattern of the missing-row related ($\sqrt{2} \times 2\sqrt{2}$) R 45° pattern, resulting at 500 K (*top*), and the c(2 × 2) pattern, resulting at 300 K (*bottom*). The missing row reconstruction leads to a smaller compressive stress change as compared to the c(2 × 2) phase

Theory can tell us about the absolute surface stress of both the clean and adsorbate-covered surface, and it is only due to this combined effort that we can judge the role of surface stress for the missing row reconstruction properly. Indeed our calculations show that the absolute value of surface stress of the c(2 × 2) phase is lowered from $-1.18\,\mathrm{N/m}$ to an average value of $-0.14\,\mathrm{N/m}$ for the two structural domains of the missing row reconstruction of Cu(100). This finding supports the view that compressive stress relief plays a role for the missing row reconstruction. Thus, the missing row reconstruction provides an alternative to the p4g clock reconstruction to lower compressive surface stress.

The calculated stress values show that the compressive stress between the c(2 × 2) and the missing row reconstruction differ by $1.04\,\mathrm{N/m}$, whereas the experimental values differ by only $0.4\,\mathrm{N/m}$. We ascribe the smaller experimental stress difference to the impact of stress relief at stress domain boundaries. STM studies of the c(2 × 2) phase indicate very small domains with abundant domain boundaries. Structural domains are also found for the missing row reconstruction, and consequently we need to consider stress relief at the domain boundaries. Overall we expect that the stress measurement give the proper sign of the O-induced surface stress change, but inter-domain stress relief leads to smaller experimental stress values as compared to the calculations.

Our calculations indicate a tensile surface stress of $+1.89\,\mathrm{N/m}$ of the clean Cu(100) surface [23]. Note, that if we had taken this stress value as a reference to convert the measured stress changes into an absolute surface stress, then we had erroneously concluded from our experimental stress data that the missing row reconstruction leads to a tensile surface stress, which is larger than the surface stress of the c(2 × 2) phase, in contrast to our discussion above. However, for this system the comparison between the clean and O-covered phase is not appropriate as it neglects the important role of structural domains for the resulting stress relief at domain boundaries.

Open questions still arise from the comparison between Ni(100) and Cu(100). Why does the former show a p4g reconstruction, whereas a missing row reconstruction is found for the latter? Why does the same O-coverage induce a re-

construction for the latter, but leads to a c(2 × 2) phase on the former substrate? Presently our understanding of the underlying mechanisms is too limited to offer simple explanations. More experimental and theoretical work is called for to advance with the understanding of the relevant processes.

4 Magnetoelastic stress of ferromagnetic monolayers

An important aspect for the successful application of ferromagnetic films for applications as sensors and data storage devices is the detailed understanding of the so-called magnetic anisotropy [9]. Magnetic anisotropy describes that certain magnetization directions of a ferromagnetic sample are energetically more favorable than others. The easy magnetization direction, i.e., the direction along which the smallest energy needs to be applied to obtain saturation magnetization, results from a competition between different contributions to the magnetic anisotropy. These contributions are either due to dipolar interactions or spin–orbit coupling. Whereas the former is the difference of stray field energies for different magnetization orientations, the latter results from subtle interactions within the spin-dependent electronic band structure. Here we show that new quantitative data on the strain dependence of the spinorbit coupling based magnetic anisotropy are obtained from stress measurements during magnetization changes.

The coupling between lattice strain and magnetism is known as magnetostriction [35], which is the change of length of a sample upon magnetization, as schematically depicted in Fig. 3. The resulting strain is usually small, and it reaches a magnitude for bulk ferromagnetic samples of the order of 10^{-5}. The inverse effect (Villari effect) describes how an externally applied strain changes the magnetization direction of a ferromagnetic sample. In short, a sample that expands upon magnetization along the magnetization direction (e.g., Fe) favors a magnetization direction parallel to an external tensile strain, and one observes a strain-induced anisotropy. The magnetoelastic coupling coefficients B_i describe this relation between strain and magnetic anisotropy, and these are the same coefficients that determine also magnetostriction [5, 35].

The magnetoelastic coupling coefficients B_i couple the strain ε_{ij} to the magnetoelastic magnetic anisotropy energy density f_{me}, as given by the following expressions for cubic and hexagonal systems, respectively [9, 28]:

$$f_{\mathrm{me}}^{\mathrm{cubic}} = B_1(\varepsilon_{11}\alpha_1^2 + \varepsilon_{22}\alpha_2^2 + \varepsilon_{33}\alpha_3^2) + B_2(2\varepsilon_{12}\alpha_1\alpha_2 + 2\varepsilon_{23}\alpha_2\alpha_3 + 2\varepsilon_{23}\alpha_2\alpha_3) + \ldots \quad (1)$$

$$f_{\mathrm{me}}^{\mathrm{hex}} = B_1(\varepsilon_{11}\alpha_1^2 + 2\varepsilon_{12}\alpha_1\alpha_2 + \varepsilon_{22}\alpha_2^2) + B_2(1-\alpha_3^2)\varepsilon_{33} + B_3(1-\alpha_3^2)(\varepsilon_{11}+\varepsilon_{22}) + B_4(2\varepsilon_{23}\alpha_2\alpha_3 + 2\varepsilon_{13}\alpha_1\alpha_3) + \ldots \quad (2)$$

The α_i are the direction cosines of the magnetization direction with respect to the crystalline axes. The dots indicate, that we have omitted higher order contributions in strain ε for clarity. However, these contributions are decisive for epitaxially strained systems discussed below, as they induce the experimentally found dependence of B on lattice strain, i.e., $B = B(\varepsilon)$.

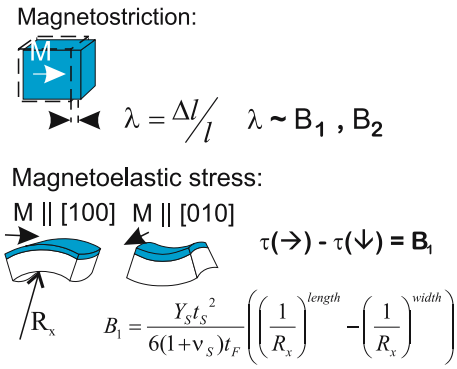

FIGURE 3 Schematic of magnetostriction of a bulk sample (*top*) and magnetoelastic stress of a film-substrate composite (*bottom*). An in-plane reorientation of the magnetization from [100] to [010] of a cubic film induces a curvature change along the sample length, which is proportional to the magnetoelastic coupling coefficient B_1

In contrast to bulk samples, ferromagnetic films are not free to strain upon magnetization due to the bonding to the substrate. Here the magnetization of the films induces a magnetoelastic stress, which can be measured from the stress-induced curvature of a thin substrate, as shown in Fig. 3. We perform experiments to determine the magnetoelastic stress from a crystal curvature measurement in a magnetic field. We work with epitaxial thin films, and the magnetoelastic coupling coefficients B_i are determined from the magnetoelastic stress, as summarized for various crystallographic orientations in Table 1 [9, 28].

There are two experimental challenges which need to be addressed when performing magnetoelastic stress measurements: the magnetoelastic stress given by B_i is in general three orders of magnitude smaller (MPa) than the epitaxial misfit induced film stress (GPa), and also an UHV compatible magnet system needs to be added to drive the magnetization reversal, preferably under control of additional magnetic characterization, e.g., by magnetooptical Kerr-effect (MOKE) measurements [36]. Signal-averaging and phase-sensitive detection schemes are applied to tackle the small magnitude of the magnetoelastic stress, and we can determine the magnetoelastic coupling down to a few atomic layer thin films, which corresponds to a radius of curvature as large as 1000 km.

Figure 4 shows a sketch of our UHV compatible arrangement of two magnets, one water-cooled stainless steel capsuled system inside the UHV chamber (vertical field of up to 0.1 T) and one external magnet with its yoke inside the UHV chamber, rotatable around the vertical axis and giving fields of up to 0.5 T in the horizontal direction, or normal to sample surface. The magnets are computer-controlled to give a vector magnetic field of the required magnitude and orientation. MOKE measurements are performed during the magnetoelastic stress measurements to ensure complete magnetization reversal with single domain states.

Figure 5 illustrates how magnetoelastic stress measurements are performed. A 5.6 nm thin Co(11$\bar{2}$0) film on W(100) is exposed to a small constant vertical field, leading to a sample magnetization along the sample length. The upper MOKE curve indicates that the sample magnetization switches from along the length to along the width when the horizontal magnetic field reaches appr. 20 mT, as indicated by the change of

film structure	B_{eff}
cubic, film axes along x_1, x_2	B_1
hexagonal, c-axis $\perp$ film plane	B_1
cubic, film axes rotated by 45° with respect to x_1, x_2	B_2
hexagonal, c-axis in-plane, 2 domains $\parallel x_1, x_2$	$\frac{1}{2}(B_1 - B_2 + B_3)$
hexagonal, c-axis in-plane, 2 domains rotated by 45° with respect to x_1, x_2	B_4
hexagonal, c-axis in-plane, 3 domains rotated by 120° with respect to x_1, x_2	$\frac{1}{4}(B_1 - B_2 + B_3) + \frac{1}{2}B_4$

TABLE 1 Effective magnetoelastic coupling coefficients B_{eff} as determined from an in-plane magnetization reversal of a film with the given orientation and symmetry. The B_i are defined above in (1) and (2). x_1: sample length, x_2: sample width. See [9, 28] for details

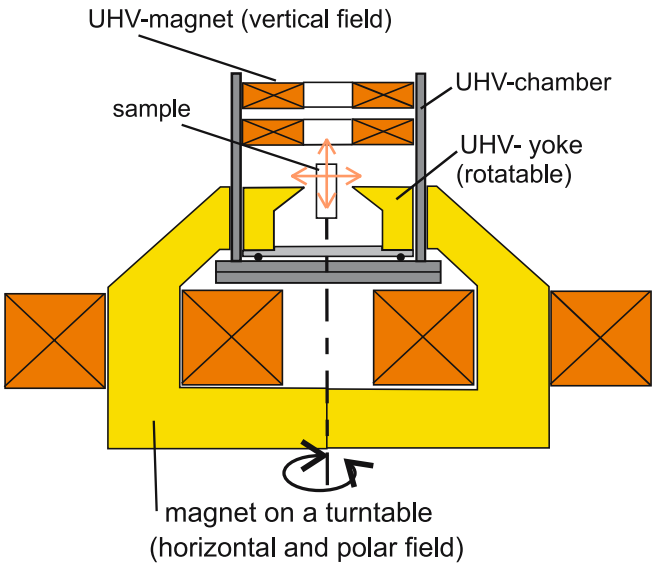

FIGURE 4 Sketch of the magnet system. The upper magnet is inside of the UHV-chamber, and it produces a vertical field, the lower magnet, which is rotatable around the vertical axis, has its coils outside of the UHV-chamber, but its yoke and pole pieces extend into the UHV chamber. The resulting vector magnetic field can be oriented in-plane or perpendicular to the sample surface

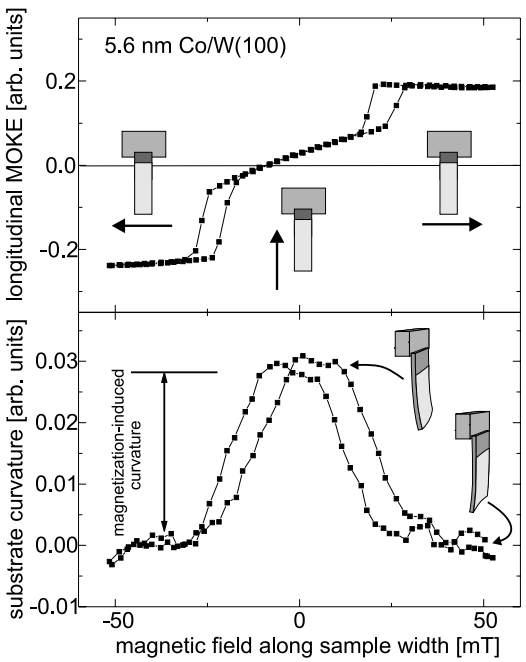

FIGURE 5 MOKE (*upper panel*) and simultaneously taken magnetoelastic stress measurements (*lower panel*) during an in-plane reorientation of the magnetization of 5.6 nm Co(11$\bar{2}$0) on W(100), measured at 300 K. The *sketches* indicate the magnetic field orientation and the sample curvature

the longitudinal MOKE signal. Simultaneously taken curvature measurements are shown in the lower panel. When the magnetization direction switches within the plane, the crystal curvature changes accordingly, and the compressive stress change indicates a negative effective magnetoelastic coupling coefficient B_4 [14]. Note that the slope of the MOKE curve around 0 mT can be exploited to determine the in-plane magnetic anisotropy [9].

The important aspect of these magnetoelastic stress measurements is that we know from our stress measurements during film growth for each film its mechanical stress. Both results, film stress and magnetoelastic stress can then be correlated by plotting the effective magnetoelastic coupling B_i^{eff} as a function of lattice strain, which we calculate from the film stress [5, 9]. The result is presented in Fig. 6.

Our results on the in situ combination of both stress measurements during film growth, which are analyzed to give the average lattice strain of a film, and magnetization-induced stress measurements, which give the magnetoelastic coupling coefficients of the deposited film clearly indicate a strain dependence of the magnetoelastic coupling, an important effect, which has also attracted theoretical attention recently [24, 25, 37–40]. Calculations of the magnetic anisotropy and of its strain dependence present a formidable task for current first principles calculations. The reason is that tiny energy differences of the order (sub-)μeV per atom determine the relevant energy differences of magnetic anisotropy calculations, and

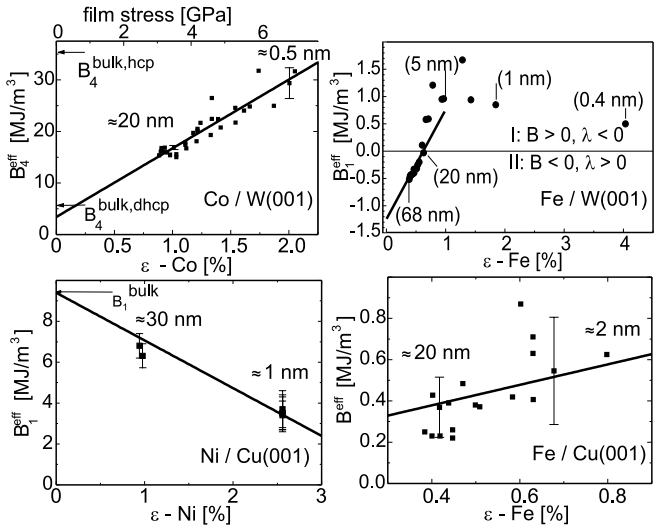

FIGURE 6 Plots of the effective B_i for different systems as a function of lattice strain ε. For all systems studied we find a non-constant behavior of B_i, and the lines through the data points are linear fits, which suggest a strain dependence of $B = B(\varepsilon)$

this requires highly accurate numerical calculations. This is illustrated by the discrepancies between theory and experimental values on bulk magnetostriction [41], not to mention the strain dependence of the magnetoelastic coupling [40].

Here, magnetoelastic stress measurements deliver important experimental reference data for upcoming theoretical work.

Our results help to disentangle the in general non-trivial competition between different contributions to the magnetic anisotropy of nanometer thin films. We find that the lattice strain, which is due to the lattice misfit between ferromagnetic film and single crystalline substrate, leads to a significant modification of the magnetoelastic coupling. This finding means that the magnetostrictive properties of a ferromagnetic sample are not constant, but vary with lattice strain.

5 Torque magnetometry by the cantilever technique

Quantitative measurements on the total magnetic moment of ferromagnetic monolayers are rare. Alternating gradient, vibrating sample and SQUID magnetometers give in principle (sub-)monolayer sensitivity, but these techniques have hardly ever been applied – most likely due to experimental obstacles – to epitaxial monolayers under UHV conditions. Only the torsion–oscillation magnetometer (TOM), modified for monolayer magnetometry under UHV in the group of Gradmann in Clausthal-Zellerfeld [42, 43], has produced a series of results on ferromagnetic monolayers. The rather limited experimental effort to obtain quantitative data on the magnetic moment of monolayers seems astonishing as interesting physics can be expected. A few examples are non-bulklike magnetic moments of interface atoms, adsorbate-induced modified magnetic moments, and induced magnetic moments in non-ferromagnetic samples at the interface with a ferromagnetic film. We demonstrate that the cantilever curvature technique presents an ultra-high vacuum (UHV) compatible way to measure magnetic moments with (sub-)monolayer sensitivity and decent accuracy in situ.

Starting point for magnetometry by the cantilever curvature technique is the mechanical torque T, which is acting on the total magnetic moment m in an magnetic field B, $\boldsymbol{T} = \boldsymbol{m} \times \boldsymbol{B}$ [44, 45]. Given a proper orientation between the vectors, the resulting torque can be exploited to induce either a curvature of a thin substrate-ferromagnetic film composite, or a deflection of a regular, i.e., thick substrate, which is suspended by a soft spring. The fist approach has been demonstrated to work well, but it requires – like in the applications of stress measurements – thin substrates (thickness 0.1 mm). Here we show, that the second approach, the suspension of a regular crystal, works as a monolayer magnetometer, and this puts little restraints on the choice and the preparation of the substrate [15].

Figure 7 shows an exploded view of the sample holder (a) and a sketch of the optical deflection measurement (b) [15]. The round Cu crystal is mounted on a thin Mo paddle (a), which serves as the soft crystal suspension to allow for the torque-induced crystal deflection. This deflection is detected by reflecting a laser beam from the crystal surface onto a position sensitive detector, as shown in (b). The Mo suspension is fabricated as a current loop, and this allows for a in situ calibration by a current I, which induces a magnetic moment m. The sample holder is mounted to a sample manipulator and transferred to a UHV glass adapter of cylinder shape, where also the magnets are positioned (not shown).

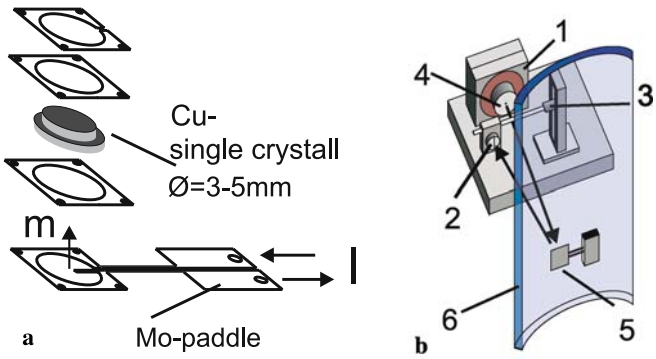

FIGURE 7 (**a**) Sketch of the crystal holder, exploded view. A current I can flow through the Mo paddle, producing a moment m, which serves as a calibration standard. (**b**) Optical deflection measurement. Outside of the UHV: 1: gimbal laser mount, 2: split photodiode as position-sensitive detector, 3: piezo-drive for deflection calibration, 4: laser, 5: sample holder in UHV, 6: UHV glass adapter

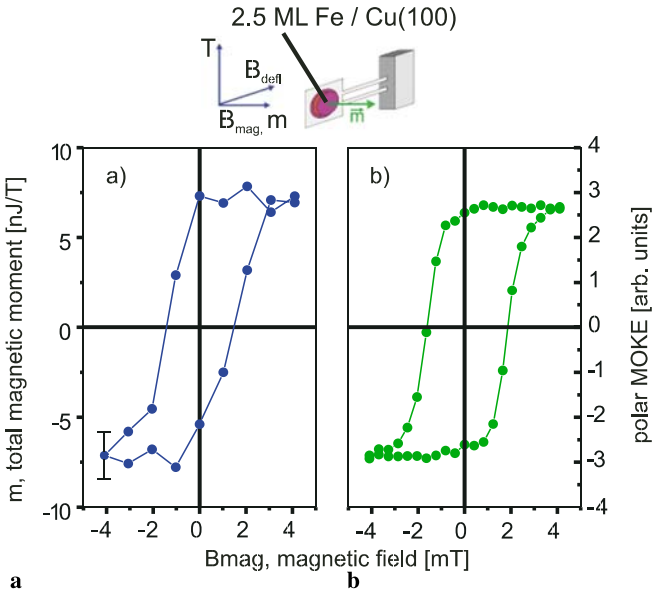

FIGURE 8 (**a**) Torque magnetometry of 2.5 ML Fe on Cu(100) at 300 K, and simultaneously measured polar MOKE (**b**). The sketch illustrates the orientation of the deflecting field B_{defl}, the magnetizing field B_{mag}, the magnetic moment m, and the resulting torque T. The total moment of 7 ± 1.3 nJ/T corresponds to $1.75 \pm 0.32\ \mu_{\mathrm{Bohr}}$ per Fe atom

Figure 8 shows a torque magnetometry measurement of 2.5 ML Fe on Cu(100). The system Fe on Cu(100) has been studied extensively in the past [46, 47], and for this Fe thickness one expects an out-of-plane magnetization of Fe. Indeed, this is what both torque magnetometry (a) and polar MOKE (b) indicate. The average magnetic moment per Fe atom is calculated from the total moment as $1.75 \pm 0.32\ \mu_{\mathrm{Bohr}}$ per Fe atom. This value is smaller than the bulk Fe moment at 300 K of $2.2\ \mu_{\mathrm{Bohr}}$. However, the Curie temperature of the 2.5 ML Fe on Cu(100) has been determined as 330 K, and we estimate that at 300 K has dropped to 72% of its saturation value. Extrapolating our value to 0 K gives a magnetic moment of $2.43 \pm 0.44\ \mu_{\mathrm{Bohr}}$ per Fe atom, in agreement with other work.

In conclusion the signal-to-noise ratio of our torque magnetometer measurements clearly indicate sub-monolayer sensitivity. The accuracy, however, is limited to roughly $\pm 18\%$. This mediocre accuracy is mainly due to the uncertainties in

the determination of the total number of Fe atoms that contributed to the torque signal. Thus, the extraction of modified magnetic moments as a function of adsorbate coverage or film thickness remains a considerable experimental challenge.

6 Conclusion

Stress measurements by the cantilever curvature technique deliver quantitative data on adsorbate-induced surface stress changes, film stress and magnetoelastic stress. These experimental data help to understand the correlation between surface stress changes and surface reconstruction, lattice misfit and film stress and film strain and magnetic anisotropy. The high sensitivity of the technique allows to detect stress changes due to sub-monolayer coverage changes. For the case of film stress measurements this means that detailed experiments on the coverage dependence of stress–strain relation of monolayer thin films are feasible. These experiments give stress values which serve as reference data for state-of-the-art calculations. The comparison between measured and calculated stress at surfaces and in monolayers is a rather unexplored field of surface science, and much less has been done here in comparison with the numerous structural investigations. In conjunction with these structural investigations one can strive for a complete description of the relevant physical principles which includes both structural and stress information at surfaces and interfaces.

The implications for the magnetic properties are evident. Magnetoelastic stress measurements present a direct way to determine the magnetoelastic coupling coefficients of ferromagnetic monolayers. The results indicate that even subtle strains in the sub-percent range can change magnitude, and also sign of the magnetoelastic coupling coefficients from their respective bulk values. This finding leads to a new understanding of the magnetic anisotropy of strained films, which goes beyond the non-justified application of bulk magnetoelastic properties also to nanoscale systems.

ACKNOWLEDGEMENTS Many experimental data on stress and torque measurements have been obtained by numerous Ph.D. students and guests of the Max-Planck-Institut. It is our great pleasure to thank Axel Enders, Thomas Gutjahr-Löser, Thomas Höpfl, Hellmut Höche, Rajapan Mahesh, Sergeij Zharkov, Wei Pan, Safia Ouazi, Zhen Tian, Amal Das, Anil Kumar for their commitment in contributing successfully to applications of the cantilever-bending technique to different topics of surface science and magnetism. We gladly acknowledge the skillful preparation of thin single-crystalline metal substrates by Heike Menge.

REFERENCES

1 H. Ibach, Surf. Sci. Rep. **29**, 193 (1997)
2 H. Ibach, Surf. Sci. Rep. **35**, 71 (1999) [Erratum]
3 R. Koch, Intrinsic stress of epitaxial thin films and surface layers, in: *The Chemical Physics of Solid Surfaces*, vol. 8 (Elsevier, Amsterdam, 1997)
4 A. Grossmann, W. Erley, H. Ibach, Surf. Rev. Lett. **2**, 543 (1995)
5 D. Sander, Rep. Prog. Phys. **62**, 809 (1999)
6 M. Hanbücken, J.P. Deville (Eds.), *Stress and Strain in Epitaxy: Theoretical Concepts, Measurements and Applications* (Elsevier, Amsterdam, 2001)
7 D. Sander, Curr. Opin. Solid State Mater. Sci. **1**, 51 (2003)
8 D. Sander, H. Meyerheim, S. Ferrer, J. Kirschner, Adv. Solid State Phys. **43**, 547 (2003)
9 D. Sander, J. Phys.: Condens. Matter **16**, R603 (2004)
10 D. Sander, Ph.D. thesis, Rheinisch-Westfälische Technische Hochschule Aachen, Mathematisch-Naturwissenschaftliche Fakultät (1992)
11 A. Grossmann, Ph.D. thesis, Rheinisch-Westfälische Technische Hochschule Aachen, Mathematisch-Naturwissenschaftliche Fakultät (1995)
12 K. Dahmen, Ph.D. thesis, Rheinisch-Westfälische Technische Hochschule Aachen, Mathematisch-Naturwissenschaftliche Fakultät (2002)
13 A. Enders, Ph.D. thesis, Martin-Luther Universität Halle-Wittenberg, Mathematisch-Naturwissenschaftlich-Technische Fakultät (1999)
14 T. Gutjahr-Löser, Ph.D. thesis, Martin-Luther Universität Halle-Wittenberg, Mathematisch-Naturwissenschaftlich-Technische Fakultät (1999)
15 T. Höpfl, Ph.D. thesis, Martin-Luther Universität Halle-Wittenberg, Mathematisch-Naturwissenschaftlich-Technische Fakultät (2000)
16 D. Sander, H. Ibach, in: *Numerical Data and Functional Relationships in Science and Technology*, Landolt-Börnstein, New Series, Group III: Condensed Matter, vol. 42, A 2 (Springer, Berlin Heidelberg New York, 2002), chap. 4.4, pp. 1–49
17 G.G. Stoney, Proc. R. Soc. London A **82**, 172 (1909)
18 R. Koch, H. Leonhard, G. Thurner, R. Abermann, Rev. Sci. Instrum. **61**, 3859 (1990)
19 Andeen-Hagerling Inc. USA, http://www.andeen-hagerling.com (2006)
20 D. Sander, A. Enders, J. Kirschner, Rev. Sci. Instrum. **66**, 4734 (1995)
21 P.J. Feibelman, Phys. Rev. B **51**, 17 867 (1995)
22 S. Stolbov, S. Hong, A. Kara, T.S. Rahman, Phys. Rev. B **72**, 155 423-1 (2005)
23 M.J. Harrison, D.P. Woodruf, J. Robinson, D. Sander, W. Pan, J. Kirschner, Phys. Rev. B **74**, 165 402 (2006)
24 M. Fähnle, M. Komelj, J. Magn. Magn. Mater. **220**, L13 (2000)
25 M. Komelj, M. Fähnle, J. Magn. Magn. Mater. **238**, L125 (2002)
26 A. Brenner, S. Senderoff, J. Res. Nat. Bur. Stand. **42**, 105 (1949)
27 K. Dahmen, S. Lehwald, H. Ibach, Surf. Sci. **446**, 161 (2000)
28 K. Dahmen, H. Ibach, D. Sander, J. Magn. Magn. Mater. **231**, 74 (2001)
29 Mateck GmbH, Jülich, Germany, http://www.mateck.de (2006)
30 Surface Science Lab, DE Zaandam, The Netherlands, http://www.surface-prep-lab.com (2006)
31 R.A. Martinez, W.M. Augustyniak, J.A. Golovchenko, Phys. Rev. Lett. **64**, 1035 (1990)
32 A.J. Schell-Sorokin, R.M. Tromp, Phys. Rev. Lett. **64**, 1039 (1990)
33 J.E. Müller, M. Wuttig, H. Ibach, Phys. Rev. Lett. **56**, 1583 (1986)
34 D. Sander, U. Linke, H. Ibach, Surf. Sci. **272**, 318 (1992)
35 C. Kittel, Rev. Mod. Phys. **21**, 541 (1949)
36 S.D. Bader, J. Magn. Magn. Mater. **100**, 440 (1991)
37 M. Fähnle, M. Komelj, R.Q. Wu, G.Y. Guo, Phys. Rev. B **65**, 144 436-1 (2002)
38 M. Komelj, M. Fähnle, Phys. Rev. B **65**, 092 403-1 (2002)
39 M. Komelj, M. Fähnle, Phys. Rev. B **65**, 212 410-1 (2002)
40 M. Komelj, M. Fähnle, Phys. Rev. B **73**, 012 404 (2006)
41 R. Wu, in: *Lecture Notes in Physics: Band Ferromagnetism* (Springer, Berlin Heidelberg New York, 2001), chapt. I, pp. 46–71
42 H.J. Elmers, U. Gradmann, Appl. Phys. A **51**, 255 (1990)
43 U. Gradmann, in:*Handbook of Magnetic Materials*, (Elsevier Science, Amsterdam, 1993) vol. 7, chap. 1, pp. 1–96
44 C. Rossel, M. Willemin, A. Gasser, H. Bothuizen, G.I. Meijer, H. Keller, Rev. Sci. Instrum. **69**, 3199 (1998)
45 T. Höpfl, D. Sander, H. Höche, J. Kirschner, Rev. Sci. Instrum. **72**, 1495 (2001)
46 J. Thomassen, F. May, B. Feldmann, M. Wuttig, H. Ibach, Phys. Rev. Lett. **69**, 3831 (1992)
47 T. Bernhard, M. Baron, M. Gruyters, H. Winter, Phys. Rev. Lett. **95**, 087 601 (2005)